IEEE Access
Multidisciplinary | Rapid Review | Open Access Journal

Received October 15, 2020, accepted October 25, 2020, date of publication November 18, 2020, date of current version February 17, 2021.

Digital Object Identifier 10.1109/ACCESS.2020.3039014

Design and Development of a Vertical Propagation Robot for Inspection of Flat and Curved Surfaces

RIZUWANA PARWEEN, (Member, IEEE), TAN YEH WEN, AND MOHAN RAJESH ELARA
Engineering Product Development Pillar, Singapore University of Technology and Design, Singapore 487372

Corresponding author: Rizuwana Parween (rizuwana_parween@sutd.edu.sg)

This work was supported in part by the National Robotics Programme under its Robotics Enabling Capabilities and Technologies under Project 192 25 00051, and in part by the administered by the Agency for Science, Technology and Research.

ABSTRACT This paper introduces a wheel-based vertical propagation robot, *Ibex*, for visual inspection of both flat and curved surfaces. The platform is modular, consisting of vacuum-based adhesion modules and steerable-wheel locomotion modules. The adhesion module consists of a unconventional design of suction cup with sufficient structural flexibility and single-axis translation freedom that helps with adhesion to flat and curved vertical surfaces. Through experiments, we validate the locomotion, adhesion, and conformation mechanisms of the robot, and collated data of the adhesion module such as differential pressure as well as normal force measurements using force sensitive resistors and a thrust force meter. We show that the platform has ability to generate a considerable amount of adhesion force while demonstrating the ability to adhere to and move on variables types of surfaces as well as various surface curvatures including plastered cement pillars and aircraft skins.

INDEX TERMS Vertical wall climbing, curved and flat wall, wheel locomotion, suction mechanism, flexible suction cup.

I. INTRODUCTION

Vertical climbing robots as a class have been an emerging field of study, especially due to the non-planar surfaces requiring various types of services such as inspection and maintenance. Such surfaces include aircraft skins [1]–[3], ship hulls [4], pipes [5], cables [6], and wind turbine blades [7]. The various services for these surfaces make human labour time consuming and dangerous, making them more suitable for vertical climbing robots to be implemented. To further work in this field, we explored current literature for curved surface propagation robots. Common mechanisms and issues detailed were collated from thirty two robot systems. As per the literature, curved surface propagation robots may be divided based on three general categories: locomotion mechanism, adhesion mechanism, and mechanisms assisting conformation to the curved surface.

In vertical robots, close contact between the robot and target surface is often necessary due to the nature of the service carried out, requiring the use of suspension mechanisms to ensure that the robot would be able to stay on the surface without falling off. Magnetism is commonly used in ferromagnetic surfaces. It is to be noted that permanent magnets were the only types of magnets used through the papers surveyed [8]–[14]. The control of the attraction force on permanent magnets is often by varying the distance between the magnets and the surface. Differential pressure [15], [16] is used as well, often involving a sealed chamber which has a lower pressure as compared to atmospheric pressure and a vacuum pump to generate the differential pressure. Such, when combined with the area over which this is exerted, results in a normal force that holds the system to the surface. There has also been use of mechanical force in order to ensure that the system will stay on the surface. Such would usually involve clamping [17], [18] or by penetrating the surface using needles [19].

While the adhesion mechanism is responsible for keeping the robot close to the surface without falling off, the locomotion mechanism ensures that the robot would be able to move on the surface while staying on it. Researchers have developed robots [15], [20]–[25] which make use of an ''alternating frame'' mechanism in order to move.

The associate editor coordinating the review of this manuscript and approving it for publication was Xiwang Dong.

These platforms typically have two parts of the body: one part remains fixed on the surface, while the other moves before attaching at a new location. The roles of the fixed part and the moving part alternate, resulting in locomotion. Parallel displacement of frames [22], [23] (the planar translation of the frames relative to one another), rotational displacement of frames [15], [24] (referring to how the frames are translated from one another relative to a common rotation axis), continuum mechanisms [26] and parallel mechanisms [25], [27] are used to achieve this. There are also robots which use legs to move. If alternating frame mechanisms is defined as having a bulk of the body to move while a certain portion stays fixed on the surface, legged mechanisms move only the limbs while the main bulk of the body remains relatively fixed on the surface [19]. Dual-wheel differential steering [16] and omnidirectional wheels [13] are among the most common wheel configurations observed in curved surface propagation robots. Other wheel configurations include dual-wheel bicycle steering [28], and four-wheel steering [4], and three-wheel synchro-drive steering [29]. Apart from wheels, track systems have also been used [30], [31].

Lim *et al.* developed an inspection robot which makes use of ropes to hoist the robot along the blade. The robot is capable of conforming to the surface of the blade using ''two linear adaptive guide actuators'', ensuring that the guide wheels remain attached on the system [32]. Wang *et al.* developed a system which makes use of electrostatic adhesion both as the means of adhesion and the means of locomotion [30]. Using three-phase AC voltage, the track moves. Using the same voltage, the system adheres to the surface as well. Use of passive joints in the system allows the robot to conform to various curvatures which it is moving on.

What distinguishes vertical curved surface robots from vertical climbing robots is the ability to conform to the curved surface. Conformation mechanisms are developed to ensure that robot systems would adhere to and move on the surface more effectively, resulting in greater surface coverage as compared to robots which do not have such mechanisms. These can be divided into three general ways, namely precise positioning, structural conformation, or structural fit. Precise positioning is defined as having the robot positioning various parts of the system in order to conform to the surface. This is usually done together with a clamping mechanism [5], [18]. Structural conformation is defined as the structure of the robot changing its shape in order to conform to the curved surface. Unlike precise positioning, structural conformation is passive. This can be done through the use of compliant mechanisms [13], free joints [28], [33], [34] or suspension systems [7]. Structural fit is defined as the structure of the robot remaining rigid as the robot is conforming to the structure. The most common design seen is V-shaped grippers, which help to position the robot as the grippers close around the surface [35]. A proof of concept system developed by Unver *et al.* was intended for smooth to relatively rough surfaces [24]. The tacky footpad foam, made out of ''a polyurethane V 10 flat elastomer'', acts as a compliant mechanism, while a ''compliant rocker mechanism with a limited motion range'' is used to further conform to the surface. The robot was able to adhere to a curvature of 1.5m diameter.

Despite the advancements made in vertical curved surface climbing robots observed from the above literature, there are several issues which current robots face. In the design considerations of our proposed robot, we have focused on some of the improvements we have made to the issues which we have identified. One design considerations is to adhere to various types of surfaces, including non-ferromagnetic surfaces without any damage to the structure. Magnets would not be useful in non-ferromagnetic structures, and penetration methods will potentially damage the structure, leaving vacuum suction, clamping, and microscopic forces. The next design consideration is for the robot to handle flat surfaces as well as surfaces of various curvatures. This would effectively eliminate clamping methods. Due to the ability of vacuum suction mechanisms to deal with any kind of surface cleanliness, vacuum suction was chosen. To deal with the various curvatures, we decided to use a flexible suction cup which would conform to various types of curvatures. Another design consideration is to minimise slippage caused by mechanical issues. Primarily, it was observed that vibrations in the system and discontinuity in movement would cause slippage. In order to reduce both issues, we have decided to use normal wheels over legs as well as omnidirectional wheels. While the use of normal wheels over legs would prove a disadvantage in obstacle climbing, nonetheless, we are assuming locomotion on a smooth to minimally rough continuous curved surface, making obstacle avoidance needless at this stage. Furthermore, wheels are faster than legs in terms of distance coverage.

Based on the design considerations, Ibex, a vertical wall climbing vision-based inspection robot for flat and curved surfaces, is developed. The platform consists of two primary modules: the adhesion module as well as the locomotion modules. These modules may be joined together using various types of hinges in order to create different configurations for various purposes. The remainder of the paper is organised as follows. Section 2 outlines the robot architecture including the mechanical and electronics design. Section 3 outlines the structural analysis of the system. Section 4 details the experimental procedures for the adhesion of the impeller on various surfaces. Section 5 discusses the experimental results.

II. ROBOT ARCHITECTURE

The Ibex platform consists of a single locomotion module with two adhesion modules, shown in Fig. 1. The exploded view the suction module and locomotion module is shown in Fig. 2 and Fig. 3, respectively. As mentioned, these modules may be joined together using various types of hinges in order to create different configurations for various purposes, though for the purposes of this paper we will be focusing on a 1-locomotion, 2-adhesion module configuration.

The adhesion module, shown in Fig. 2, comprises of four main components: the main suction chamber, suction cup,

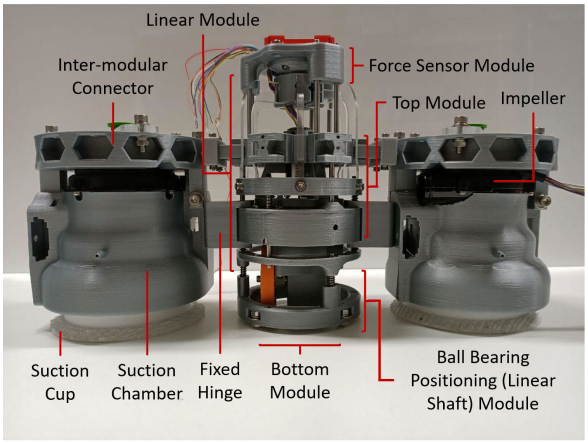

FIGURE 1. Ibex- the vertical robot platform (Configuration 1-2).

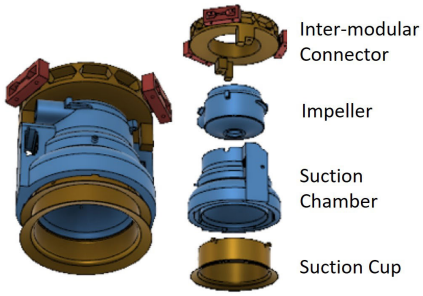

FIGURE 2. Exploded view of the suction module of the platform.

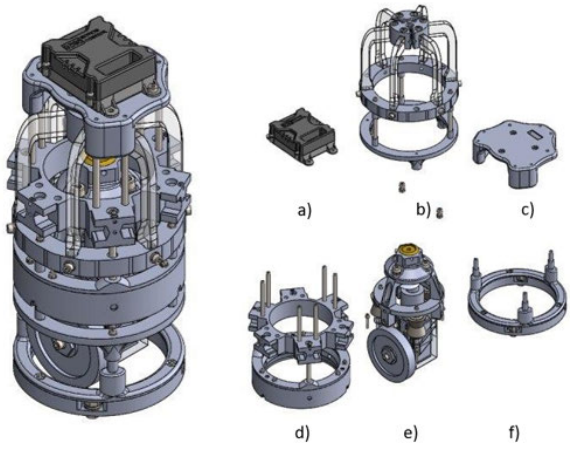

FIGURE 3. Locomotion module of the Ibex platform and exploded view of the locomotion module of the Ibex platform. The various modules in order: a) Roboclaw 2 × 7A b) Linear Module c) Force Sensor Module d) Top Module e) Bottom Module f) Ball Bearing Positioning (Linear Shaft) Module.

impeller, and inter-modular connector. The impeller generates pressure difference between the inner chamber and atmospheric pressure. The inter-modular connector allows the module to be connected to other modules according to the setup required. The main suction chamber, made with PLA, serves to maintain the pressure difference as well as to restrict the movement of the suction cup to one DOF. It allows the suction cup to move in one axis up to 2cm without rotation. The suction cup, made with TPU, is flexible enough in order to adapt to various types of surface curvature. The suction cup is equipped with a skirt which serves to maintain the pressure difference in the chamber and to generate a normal force for the suction cup to remain attached on the surface. Preliminary studies on this design showed that the suction cup would remain attached to the surface even though the suction chamber is pulled away from the adhesion surface, reinforcing the feasibility of the design.

The main suction chamber and the suction cup were separated in order to ensure that most of the normal force being exerted on the adhesion module would be focused on the suction chamber rather than on the suction cup. As the suction chamber would be directly connected to the locomotion module, it implies that most of the normal force would be acting on the locomotion module. Such a design is crucial as we want the frictional force of the cup and the wheel, which are directly related to the normal force experienced by both the suction cup and the suction chamber, to be as small and as large as possible respectively. This is to ensure locomotion on the surface as well as to prevent the robot from slipping and falling. Two differential pressure sensors (AMS5915-0100-D-B from NCD) can be added at the sides to track the pressure difference.

The locomotion module comprises of five main sections: the driving section, rotary section, linear section, force feedback section, and inter-modular section, shown in Fig. 3. The driving section generates the driving force. This is connected to the rotary section, allowing the driving section to rotate freely or with the assistance of a motor. Encoders are proposed to be connected by a bevel gear system in order to track the angular position of the wheel, while an additional motor will control the position. It is to be noted that the wheel is currently a distance from the rotary axis. This is inspired by CityClimber [36] in order to reduce damage to the wheel when the wheel is rotating about the axis. The linear section connects the rotary section to the force feedback section. The design consideration behind this is to ensure to allow only one DOF between the rotary section and the force feedback section. This would allow us to reliably detect the normal force acting on the wheel. Like in the adhesion module, the inter-modular section allows for connections to other modules.

The electronics block diagram of the platform is shown in Fig 4. Each wheel module is equipped with a wheel mounted on a CHIHAI GM4632-370 DC motor. A Pololu Micro Metal Gearmotor will control the steering of the motor. Both motors in each wheel will be connected to a motor controller, RoboClaw 2 × 7A Motor Controller (V5C). In order to ensure full rotation of the wheel, the wires of the CHIHAI motor are linked to the Roboclaw controller via a slip ring in order to ensure that the wires would not be tangled. Each Roboclaw 2 × 7A, defined with a unique address, will communicate with the micro-controller (Arduino Mega 2560 16-bit) serially. The serial communication between the micro-controller and motor controller is full duplex which enables motor controller to send encoder

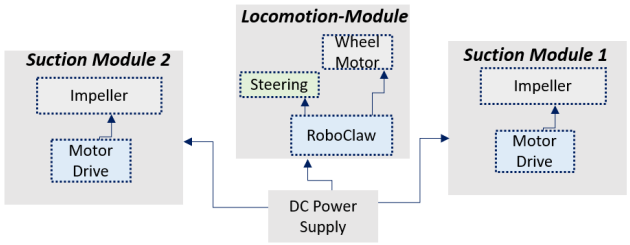

FIGURE 4. Block diagram of the electronics module of the Ibex platform.

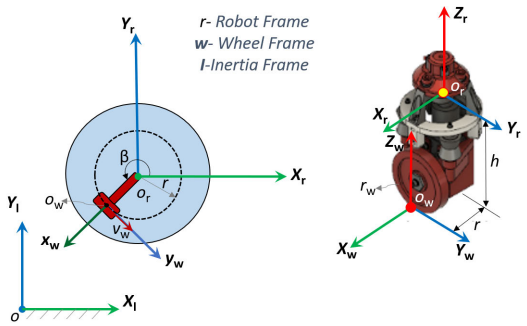

FIGURE 5. Schematic of the kinematic diagram showing the coordinate frame.

feedback from the motors to Arduino and receive the control signals from Arduino to drive the DC motors simultaneously.

III. MODELLING AND ANALYSIS

A. KINEMATIC MODELING

In this section, the wheel position in inertial frame formulated based on the composite homogeneous transformation matrix between the robot frame and inertial frame is formulated. Figure 5 shows the schematic diagram of the wheel layout, used for kinematic formulation.

$\dot{\phi}$ = Wheel Speed;

r_w = Wheel Radius;

o_w = The point of contact of the wheel on the wall surface;

o_r = CG location of the platform;

r = Offset distance of the Wheel from the CG; h = Gap between the wall and CG;

x_c, y_c, z_c = position of the point of contact of the wheel in the inertial frame, respectively;

β = Steering angle of the wheel;

θ = Heading angle;

The wheel position in the inertial frame is given by

$$\begin{bmatrix} x_w \\ y_w \\ z_w \\ 1 \end{bmatrix} = \begin{bmatrix} \cos\theta & -\sin\theta & 0 & 0 \\ \sin\theta & \cos\theta & 0 & 0 \\ 0 & 0 & 1 & 0 \\ 0 & 0 & 0 & 1 \end{bmatrix} \begin{bmatrix} \cos\beta & \sin\beta & 0 & -r \\ -\sin\beta & \cos\beta & 0 & 0 \\ 0 & 0 & 1 & h \\ 0 & 0 & 0 & 1 \end{bmatrix} \quad (1)$$

The locomotion of the platform is performed by actuating the wheel DC motor and steering motor. By regulating both wheel motor and steering motor, the platform can move forward, back, and turn. The robot has three degree of freedom which are given by pose of the robot and robot heading. The robot pose and heading can be controlled by two control inputs and hence the system represents a underactuated system. For the navigation on the flat and curved wall, we use unicycle based kinematics. Let v_p and ω_p are the linear velocity and angular velocity of the robot platform about its CG respectively. The kinematics is given by the following Equation.

$$\begin{aligned} v_p &= r_w\dot{\phi} \\ \dot{x}_c &= v_p\cos(\theta+\beta) \\ \dot{y}_c &= v_p\cos(\theta+\beta) \\ w_p &= \dot{\theta} = \dot{\beta} \end{aligned} \quad (2)$$

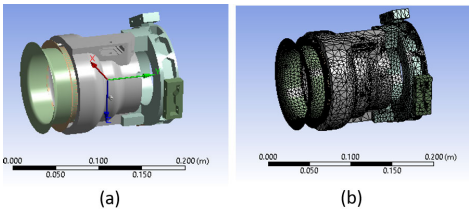

FIGURE 6. (a) CAD and (b) meshed model of the suction module.

B. FINITE ELEMENT BASED STRUCTURAL ANALYSIS

Natural frequency is a critical parameter of any oscillating system. If the oscillating system is driven by an external force at the natural frequency of the system, then the system is under resonance and fail. Even though the structural platform of the robot is made rigid, cleaning pay load and friction on the surface may add additional load to the motor and cause failure due to resonance. Therefore, during locomotion and transformation, the actuation speed of the motors attached to wheels and the hinged joints must be set less than the natural frequency of the system to avoid the structural resonance. Three dimensional CAD model of the structural platform is built, as shown in Figure 6. A frequency (modal) analysis of the platform is carried out in ANSYS Workbench. For this analysis, the material properties including density, elastic modulus, Poision's ratio are considered as 1.24 g /cm^3, 0.3, and 3.36 GPa, respectively. With these material, boundary and load settings, a modal (free vibration) analysis is carried out in Workbench environment to obtain the natural frequencies and mode shapes of the platform. The first three natural frequencies are as shown in Figure 7. The first two natural modes represents the symmetrical bending body modes of the platform. The third mode represents the torsional mode shapes. During suction and locomotion, the driving frequency of the impeller and wheel must be set below the first natural frequency to avoid the structural failure.

A static structural analysis is carried out in Workbench environment to study the the gravitational (1g) effect on the suction module. A payload of 2.5 kg is applied as a uniformly distributed load on the platform. Fixity boundary

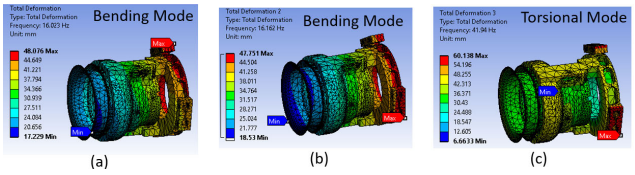

FIGURE 7. Mode shapes of the suction module during free vibration (a) 1st mode, (b) second mode, (c) third mode.

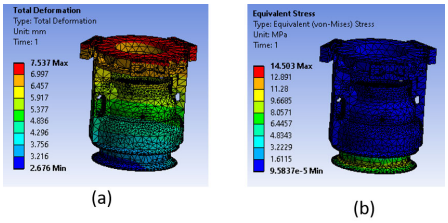

FIGURE 8. (a) Static deformation and (b) Stress pattern in the suction module.

condition is applied at the ground-wheel contact point of the platform. The deformed components of suction module is shown in Figure 8(a). The maximum deformation is 7.5 mm, which occurs near the distant edge suction module. This deformation is approximately equal to the one-tenth of the critical dimension (8 cm) of the platform. Figure 8(b) presents the distribution of the stress in the suction module. Maximum stress of magnitude 14.5 MPa, occurs near the wheel support which is lower than the tensile stress of PLA (40 MPa). Therefore, the current platform design is considered to be safe under static condition.

IV. EXPERIMENTAL PROCEDURE

To validate the adhesion, conformation, and locomotion mechanisms of the robot, experiments were carried out to study the adhesion module. This would allow us to understand the performance of the adhesion module on various surfaces, as well as to validate whether most of the normal force is acting on the suction chamber rather than on the suction cup. Furthermore, a robot configuration was tested in order to understand locomotion principles.

Experiments were conducted to study the impeller module with the following experimental set up. The impeller, secured to a thrust force meter, is made to adhere to five different surfaces, as seen in Fig. 9. While the power is set to maximum on the impeller's control card, the voltage is controlled on the power source, ranging from 16V to 26V at 2V increments. The normal operational voltage of the impeller is 24V. Force sensors, shown in Fig. 10, detect the normal force exerted by the suction cup, while the normal force exerted by the suction chamber is measured by the thrust force meter. Furthermore, it is noted that the impeller module is mounted such that both the suction cup and the suction chamber is free to move independently along one axis during the test, minimising force interaction between both parts. The impeller is supported by a roller to ensure that it will remain mostly normal to the experimental surface. While the Arduino took readings from

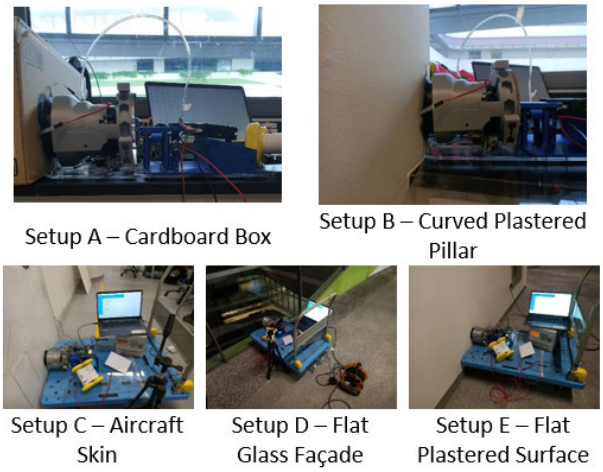

FIGURE 9. Experimental Setup in Surfaces Tested.

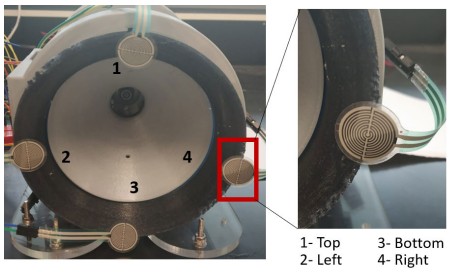

FIGURE 10. Position of Force Sensors for the estimation of the normal pressure exerted by the suction cup on various surface.

the force sensors and the pressure sensor at approximately one second intervals, an external phone camera recorded readings from the thrust force meter and power source. The video is then run through VLC Media Player to extract the frames from the video for comparison. Thrust force meter and ampere were then extracted from the video frames if either of the first two images from the first appearance of the given time is definitely clear. If both images are not clear in either reading, the data is rejected as a whole. Though there are two pressure sensor holes on the impeller module, one of the holes was connected to the pressure sensor (AMS5915-0100-D-B) while the other was sealed shut using tape in order to ensure that the pressure difference would be as close as possible to the real situation.

V. EXPERIMENTAL RESULTS

Through the experiment, we extracted normal force from the suction cup and the suction chamber, as well as differential pressure from the various surfaces. In addition, 25 equally spaced (4 seconds apart) points were taken from a pseudo-static segment, with the last point being 10 seconds or slight more away from when the system is turned off. If a particular point is not recorded by the Arduino, the data is input as N/A. Data information from this method included, in addition to the two above mentioned, current readings. The number of valid data points are listed in Fig. 11.

	A	B	C	D	E
16	10	6	16	9	3
18	13	6	2	2	14
20	6	15	2	2	17
22	16	12	2	6	3
24	10	11	20	5	9
26	6	11	5	5	2

FIGURE 11. Number of Valid Data Points from Various Surfaces at Various Voltages from A Pseudo-Static Timeframe.

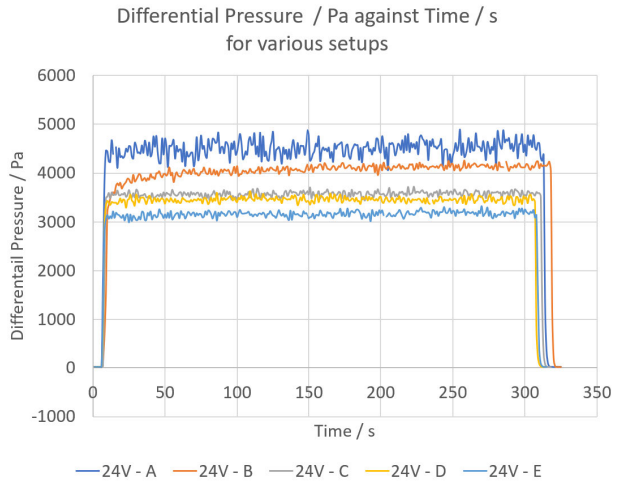

FIGURE 12. Differential pressure in the suction chamber of the Ibex platform across various systems at 24V.

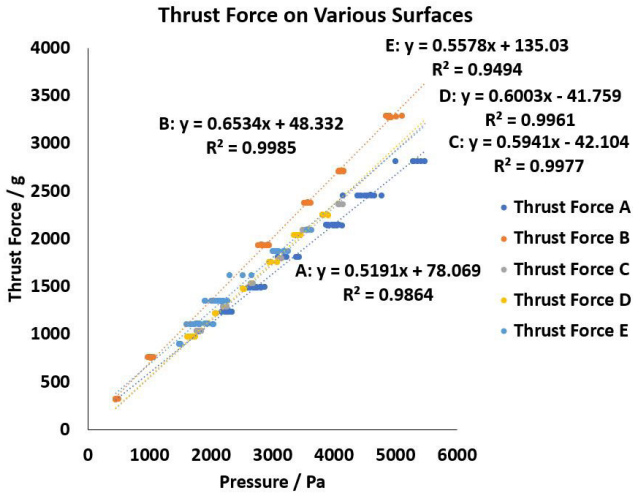

FIGURE 13. Thrust Force against Differential Pressure for all surfaces from pseudo-static state.

We analysed the data collected from the experiment setup in order to check if the design considerations for the adhesion and locomotion modules are validated, as well as to gather information about the system that could be used to control the system in future works.

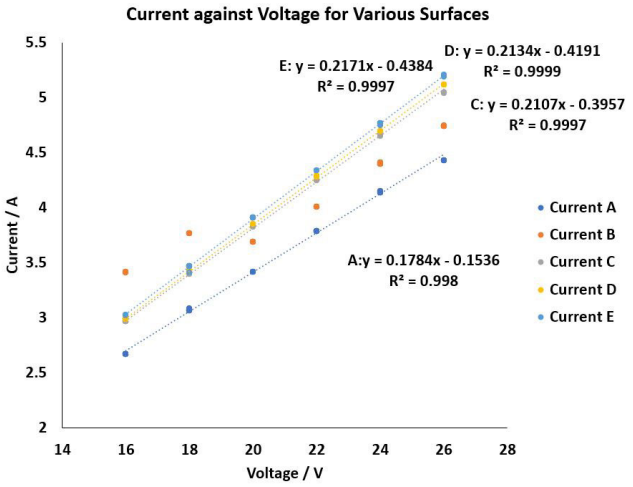

FIGURE 14. Current against Voltage for all surfaces from pseudo-static state.

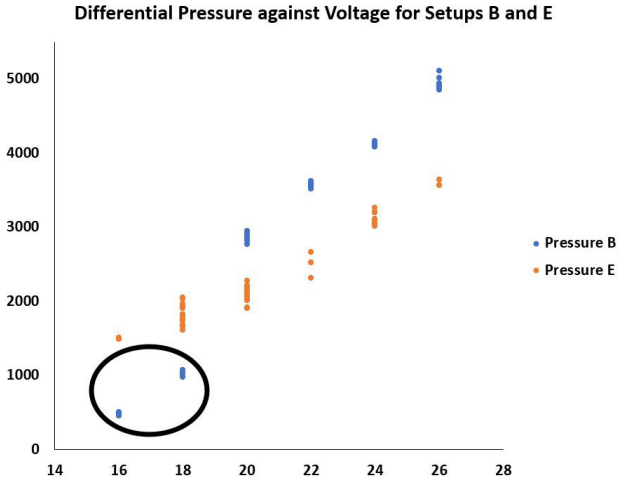

FIGURE 15. Differential Pressure against Voltage for Setups B (Curved Plastered Cement Pillar) and E (Flat Plastered Cement Wall).

A. DIFFERENTIAL PRESSURE IN THE SUCTION CHAMBER ACROSS VARIOUS SETUPS

Figure 12 highlights how the various surfaces affect the differential pressure in the chamber at 24V, which is the normal operational voltage supplied to the impeller. It is to be noted that Setup A, being the cardboard box, had the highest differential pressure, possibly due to the deformation of the cardboard box resulting in the surface being closer to the impeller than expected. However, it is also the noisiest, possibly because the deformation of both the cup and the cardboard resulted in greater air gaps between the two surfaces. It is interesting to see that the two plastered surfaces, Setup B and Setup E were respectively the second highest and the lowest. One might expect that for the same type of surface, the curved surface would be the one with lower differential pressure. One might venture a guess and say that Setup E was dirtier than Setup B, and hence it affected the performance of the impeller. Setup B takes the longest to stabilise. This can be

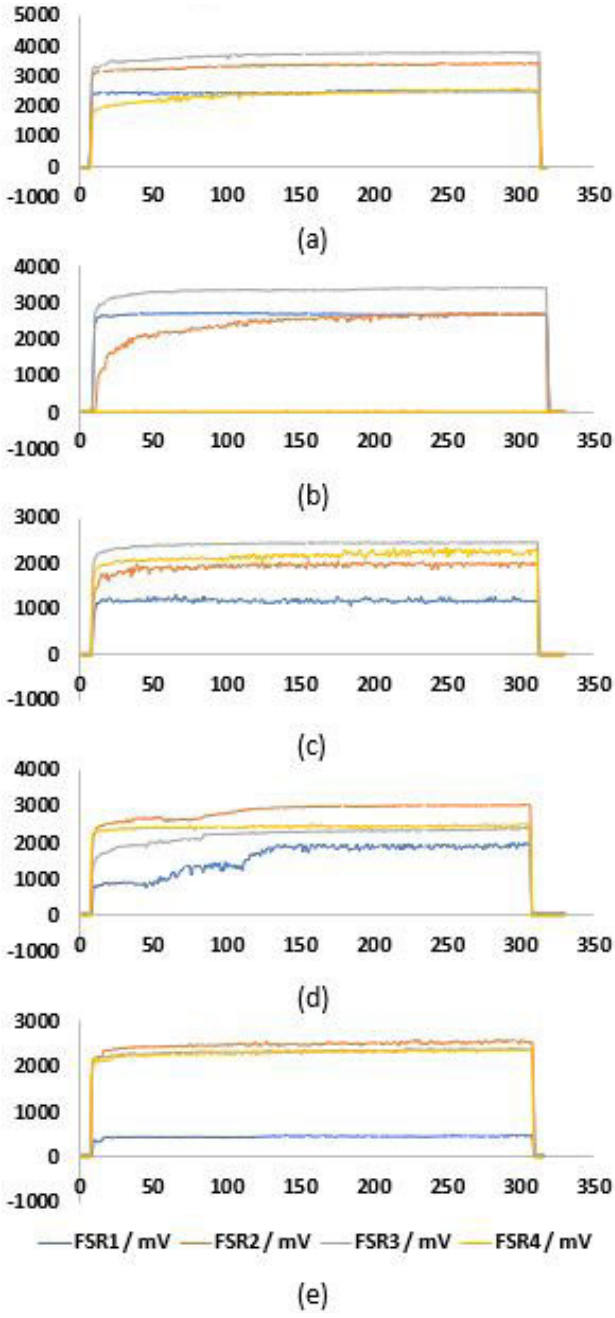

FIGURE 16. Suction cup force sensor readings (a) Setup A: Cardboard (b) Setup B: Curved plastered cement pillar (c) Setup C: Aircraft skin (d) Setup D: Flat plastered cement pillar (e) Setup E: Flat glass facade. Voltage supplied at 24V.

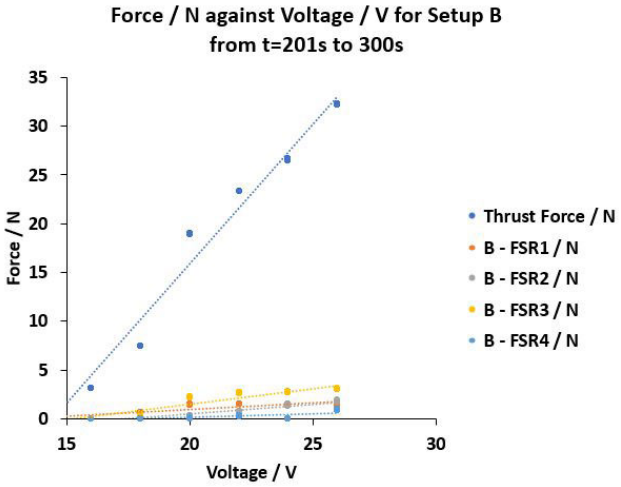

FIGURE 17. Force readings from suction cup force sensors and thrust force meter at various voltages in Setup B.

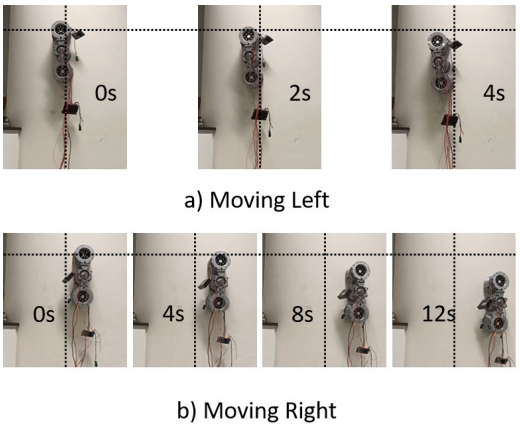

FIGURE 18. Locomotion on Curved Pillar with Timestamps.

understood as the suction cup requiring some time in order to conform to the curved surface.

Figure 13 shows force and pressure data from points from all the setups from the pseudo-static period extracted and compared to see if there is a correlation between differential pressure and thrust force when the system is stabilised. Through this, a clear linear correlation between both differential pressure and thrust force with the voltage supplied to the system was observed for all the surfaces, making differential pressure a potential candidate for closed-loop feedback control.

It is to be noted that the gradients for setup A and B are different from setups C, D, and E. For setup A, one of the reasons could be attributed to the deformability of the cardboard box. For setup B, being the surface with the greatest curvature, it is possible that the effective suction area has changed due to the deformation of the cup, and is of interest for future research.

Figure 14 shows current and voltage data from points from all the setups from the pseudo-static period extracted and compared to see. Ideally, a clear linear correlation between the current and voltage should be observed due to Ohm's Law. While we do observe for most of the setups, we observe that there is a discontinuous jump for setup B. This could be linked to the curvature of the surface, where at the lower voltages, the differential pressure is insufficient to keep the cup adhered to the surface, resulting in an incomplete sealing, and hence a current spike. This reasoning is in line with how there is a large jump between the pressure differences from 18V to 20V while a wall of similar material and covering does not have such a jump as shown in Fig. 15 (circled).

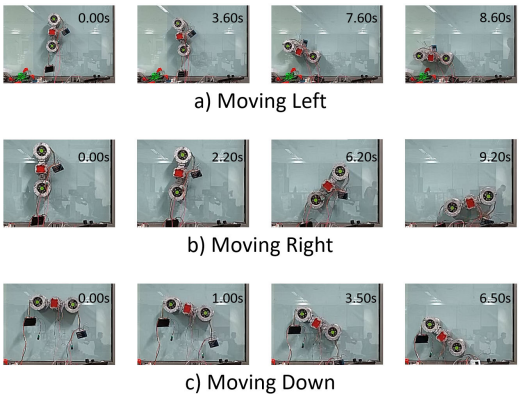

FIGURE 19. Locomotion on Flat Window with Timestamps.

We also note that setup A's gradient is different from setups C, D, and E, which are close to one another. This is particularly of interest because we do not expect the resistance of the impeller to change throughout the experiments. This is of future research interest as well.

In Figure 16, we see that the suction cup experiences a normal force on all the force sensors during the experiment in various setups. This proves that the suction cup is adhering to the surface, despite varying curvatures and roughness of the surfaces.

As an example, in Fig. 17, we compare the forces exerted on the suction chamber and the suction cup over various voltages supplied to the impeller in setup B. Through this, we validate that most of the normal force is acting on the suction chamber rather than the suction cup.

VI. LOCOMOTION CAPABILITY

With the adhesion module tested and validated, it is safe to test a robot configuration. A 1-locomotion, 2-adhesion configuration (1-2 configuration) was assembled and tested on a curved pillar and a window. Figure 18 and Figure 19 show locomotion on the respective surfaces. The driving module in the locomotion module was fixed perpendicular to the robot body throughout locomotion. Through this, Ibex demonstrated capabilities of moving on continuous flat and curved surfaces, as well as on smooth to minimally rough surfaces.

VII. CONCLUSION AND FUTURE WORK

In this paper, we have presented a novel design of curved surface vertical climbing robot, with a vacuum-based adhesion module and a steerable wheel locomotion module. The adhesion module consists of a flexible suction cup which is able to conform to various types of curvatures. We have also carried out finite element analysis to check the structural performance of the suction module. Through the experiments, we are able to validate the locomotion, adhesion, and conformation mechanisms of the robot. We were able to validate the feasibility of adhering on smooth to minimally rough surfaces of various curvatures through our adhesion module. Furthermore, we were able to show the feasibility of locomotion on various surfaces using said adhesion module and locomotion modules.

It is to be noted that some points of interest were not able to be recorded using the data extraction method detailed. For example, it is noted that the ampere reading will first reach a peak before coming down to a stable value, which could be related to when the pressure was being generated in the chamber, and subsequently the thrust force as well. However, for purposes regarding the stability of the system when the impellers are in motion, the data extracted is sufficient. With the extracted data, closed feedback control of the differential pressure in order to control the normal force acting on the system will be explored. Further studies can also be done to see how the surface curvature affects the time required for the differential pressure to be stabilised. Other future work includes investigating payload capacity, navigation and control of the robot extended to other surfaces, as well as integrating an inspection module.

REFERENCES

[1] M. A. V. J. Muthugala, M. Vega-Heredia, R. E. Mohan, and S. R. Vishaal, "Design and control of a wall cleaning robot with adhesion-awareness," *Symmetry*, vol. 12, no. 1, p. 122, Jan. 2020.

[2] B. Ramalingam, V.-H. Manuel, M. R. Elara, A. Vengadesh, A. K. Lakshmanan, M. Ilyas, and T. J. Y. James, "Visual inspection of the aircraft surface using a teleoperated reconfigurable climbing robot and enhanced deep learning technique," *Int. J. Aerosp. Eng.*, vol. 2019, pp. 1–14, Sep. 2019.

[3] J. Gu, C. Wang, and X. Wu, "Self-adjusted adsorption strategy for an aircraft skin inspection robot," *J. Mech. Sci. Technol.*, vol. 32, no. 6, pp. 2867–2875, Jun. 2018.

[4] B. Ross, J. Bares, and C. Fromme, "A semi-autonomous robot for stripping paint from large vessels," *Int. J. Robot. Res.*, vol. 22, nos. 7–8, pp. 617–626, Jul. 2003.

[5] P. Chatzakos, Y. P. Markopoulos, K. Hrissagis, and A. Khalid, "On the development of a modular external-pipe crawling omni-directional mobile robot," in *Climbing and Walking Robots*. Springer, 2006, pp. 693–700.

[6] K. H. Cho, H. M. Kim, Y. H. Jin, F. Liu, H. Moon, J. C. Koo, and H. R. Choi, "Inspection robot for hanger cable of suspension bridge: Mechanism design and analysis," *IEEE/ASME Trans. Mechatronics*, vol. 18, no. 6, pp. 1665–1674, Dec. 2013.

[7] S. Hayashi, T. Takei, K. Hamamura, S. Ito, D. Kanawa, E. Imanishi, and Y. Yamauchi, "Moving mechanism for a wind turbine blade inspection and repair robot," in *Proc. IEEE/SICE Int. Symp. Syst. Integr. (SII)*, Dec. 2017, pp. 270–275.

[8] H. Leon-Rodriguez and S. T. H. Sattar, "A compact wall-climbing and surface adaptation robot for non-destructive testing," in *Proc. 12th Int. Conf. Control, Automat. Syst.*, Oct. 2012, pp. 404–409.

[9] J. Shang, B. Bridge, T. Sattar, S. Mondal, and A. Brenner, "Development of a climbing robot for inspection of long weld lines," *Ind. Robot, Int. J.*, vol. 35, no. 3, pp. 217–223, May 2008.

[10] W. Fischer, G. Caprari, R. Siegwart, I. Thommen, W. Zesch, and R. Moser, "Foldable magnetic wheeled climbing robot for the inspection of gas turbines and similar environments with very narrow access holes," *Ind. Robot, Int. J.*, vol. 37, no. 3, pp. 244–249, May 2010.

[11] T. Sattar, M. Alaoui, S. Chen, and B. Bridge, "A magnetically adhering wall climbing wall robot to perform continuous welding of long seams and non destructively test the welds on the hull of a container ship," in *Proc. 8th IEEE Conf. Mechatronics Mach. Vis. Pract.*, Aug. 2001, pp. 408–414.

[12] S. Nansai and R. Mohan, "A survey of wall climbing robots: Recent advances and challenges," *Robotics*, vol. 5, no. 3, p. 14, Jul. 2016.

[13] M. Tavakoli and C. Viegas, "Analysis and application of dual-row omni-directional wheels for climbing robots," *Mechatronics*, vol. 24, no. 5, pp. 436–448, Aug. 2014.

[14] W. Fischer, G. Caprari, R. Siegwart, and R. Moser, "Locomotion system for a mobile robot on magnetic wheels with both axial and circumferential mobility and with only an 8-mm height for generator inspection with the rotor still installed," *IEEE Trans. Ind. Electron.*, vol. 58, no. 12, pp. 5296–5303, Dec. 2011.
[15] H. Choi, J. Park, and T. Kang, "A self-contained wall climbing robot with closed link mechanism," *KSME Int. J.*, vol. 18, no. 4, pp. 573–581, Apr. 2004.
[16] T. S. White, R. Alexander, G. Callow, A. Cooke, S. Harris, and J. Sargent, "A mobile climbing robot for high precision manufacture and inspection of aerostructures," *Int. J. Robot. Res.*, vol. 24, no. 7, pp. 589–598, Jul. 2005.
[17] M. Tavakoli, M. R. Zakerzadeh, G. R. Vossoughi, and S. Bagheri, "A hybrid pole climbing and manipulating robot with minimum DOFs for construction and service applications," *Ind. Robot, Int. J.*, vol. 32, no. 2, pp. 171–178, Apr. 2005.
[18] M. Almonacid, R. J. Saltaren, R. Aracil, and O. Reinoso, "Motion planning of a climbing parallel robot," *IEEE Trans. Robot. Autom.*, vol. 19, no. 3, pp. 485–489, Jun. 2003.
[19] G. C. Haynes, A. Khripin, G. Lynch, J. Amory, A. Saunders, A. A. Rizzi, and D. E. Koditschek, "Rapid pole climbing with a quadrupedal robot," in *Proc. IEEE Int. Conf. Robot. Autom.*, May 2009, pp. 2767–2772.
[20] L. Guo, K. Rogers, and R. Kirkham, "A climbing robot with continuous motion," in *Proc. IEEE Int. Conf. Robot. Autom.*, May 1994, pp. 2495–2500.
[21] J. Shang, T. Sattar, S. Chen, and B. Bridge, "Design of a climbing robot for inspecting aircraft wings and fuselage," *Ind. Robot, Int. J.*, vol. 34, no. 6, pp. 495–502, Oct. 2007.
[22] T. White, N. Hewer, B. L. Luk, and J. Hazel, "The design and operational performance of a climbing robot used for weld inspection in hazardous environments," in *Proc. IEEE Int. Conf. Control Appl.*, Sep. 1998, pp. 451–455.
[23] H. Zhang, J. Zhang, G. Zong, W. Wang, and R. Liu, "Sky cleaner 3: A real pneumatic climbing robot for glass-wall cleaning," *IEEE Robot. Autom. Mag.*, vol. 13, no. 1, pp. 32–41, Mar. 2006.
[24] O. Unver and M. Sitti, "A miniature ceiling walking robot with flat tacky elastomeric footpads," in *Proc. IEEE Int. Conf. Robot. Autom.*, May 2009, pp. 2276–2281.
[25] M. Tavakoli, M. R. Zakerzadeh, G. R. Vossoughi, and S. Bagheri, "Design and prototyping of a hybrid pole climbing and manipulating robot with minimum DOFs," in *Climbing and Walking Robots*. Springer, 2005, pp. 1071–1080.
[26] T. L. Lam and Y. Xu, "Biologically inspired tree-climbing robot with continuum maneuvering mechanism," *J. Field Robot.*, vol. 29, no. 6, pp. 843–860, Nov. 2012.
[27] C. Schlosser and T. Schüppstuhl, "Numerical controlled robot crawler: New resource for industries with large scale products," *Prod. Eng.*, vol. 8, no. 6, pp. 719–725, Dec. 2014.
[28] F. Tache, W. Fischer, R. Siegwart, R. Moser, and F. Mondada, "Compact magnetic wheeled robot with high mobility for inspecting complex shaped pipe structures," in *Proc. IEEE/RSJ Int. Conf. Intell. Robots Syst.*, Oct. 2007, pp. 261–266.
[29] J. Sánchez, F. Vázquez, and E. Paz, "Machine vision guidance system for a modular climbing robot used in shipbuilding," in *Climbing and Walking Robots*. Springer, 2006, pp. 893–900.
[30] H. Wang, A. Yamamoto, and T. Higuchi, "Electrostatic-motor-driven electroadhesive robot," in *Proc. IEEE/RSJ Int. Conf. Intell. Robots Syst.*, Oct. 2012, pp. 914–919.
[31] K. H. Cho, Y. H. Jin, H. M. Kim, and H. R. Choi, "Development of novel multifunctional robotic crawler for inspection of hanger cables in suspension bridges," in *Proc. IEEE Int. Conf. Robot. Autom. (ICRA)*, May 2014, pp. 2673–2678.
[32] S. Lim, C.-W. Park, J.-H. Hwang, D.-Y. Kim, and T.-K. Kim, "The inchworm type blade inspection robot system," in *Proc. 9th Int. Conf. Ubiquitous Robots Ambient Intell. (URAI)*, Nov. 2012, pp. 604–607.
[33] G. La Rosa, M. Messina, G. Muscato, and R. Sinatra, "A low-cost lightweight climbing robot for the inspection of vertical surfaces," *Mechatronics*, vol. 12, no. 1, pp. 71–96, Feb. 2002.
[34] B. L. Luk, A. A. Collie, D. S. Cooke, and S. Chen, "Walking and climbing service robots for safety inspection of nuclear reactor pressure vessels," *Meas. Control*, vol. 39, no. 2, pp. 43–47, Mar. 2006.
[35] M. Tavakoli, L. Marques, and A. T. de Almeida, "3DCLIMBER: Climbing and manipulation over 3D structures," *Mechatronics*, vol. 21, no. 1, pp. 48–62, Feb. 2011.
[36] D. Schmidt, *Safe Navigation of a Wall-Climbing Robot-Risk Assessment and Control Methods*. Dr. Hut: Plano, TX, USA, 2013.

RIZUWANA PARWEEN (Member, IEEE) received the bachelor's and master's degrees in mechanical engineering from the National Institute of Technology Rourkela, India, and the Ph.D. degree from the Indian Institute of Science, Bengaluru, India. She has over two years of industrial experience as a Product Development Engineer with KSB Tech Private Ltd., Pune, and as a Structural Analyst with CUMMINS, Pune. As a Postdoctoral Research Fellow with SUTD, she worked on the design and development of Unloader Knee Brace for Asian Patients, in collaboration with physicians in Changi General Hospital, Singapore. She is currently a Research Fellow with the Engineering Product Development Pillar, Singapore University of Technology and Design (SUTD). She is also a Research Fellow working on the design, development, and modeling of the self-reconfigurable floor cleaning robots.

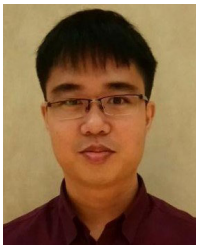

TAN YEH WEN received the B.Eng. degree in alternative energy from the Singapore University of Technology and Design (SUTD), in 2017, where he is currently pursuing the Master of Engineering (Research) degree under Prof. Mohan. He joined Prof. Mohan as a Research Assistant in his laboratory.

MOHAN RAJESH ELARA received the B.E. degree from the Amrita Institute of Technology and Sciences, Bharathiar University, India, and the M.Sc. degree in consumer electronics and the Ph.D. degree in electrical and electronics engineering from Nanyang Technological University, Singapore. He was a Lecturer with the School of Electrical and Electronics Engineering, Singapore Polytechnic. He is currently an Assistant Professor with the Engineering Product Development Pillar, Singapore University of Technology and Design (SUTD). He is also a Visiting Faculty Member of the International Design Institute, Zhejiang University, China. He has published more than 80 papers in leading journals, books, and conferences. His research interests include robotics with an emphasis on self-reconfigurable platforms as well as research problems related to robot ergonomics and autonomous systems. He has served in various positions of organizing and technical committees of over twenty international competitions and conferences. He was a recipient of the SG Mark Design Award, in 2016, 2017, and 2018, the A' Design Award, in 2018, the ASEE Best of Design in Engineering Award, in 2012, and the Tan Kah Kee Young Inventors' Award, in 2010.